Polymorphism of highly cross-linked F-actin networks: Probing multiple length scales

Lam T. Nguyen[1] and Linda S. Hirst[2]

[1]*Department of Physics & MARTECH, Florida State University, Tallahassee, Florida 32306, USA*
[2]*School of Natural Sciences, University of California, Merced, California 95344, USA*

The assembly properties of F-actin filaments in the presence of different biological cross-linker concentrations and types have been investigated using a combined approach of fluorescence confocal microscopy and coarse-grained molecular dynamics simulation. In particular for highly cross-linked regimes, new network morphologies are observed. Complex network formation and the details of the resulting structure are strongly dependent on the ratio of cross-linkers to actin monomers and cross-linker shape but only weakly dependent on overall actin concentration and filament length. The work presented here may help to provide some fundamental understanding of how excessive cross-linkers interact with the actin filament solution, creating different structures in the cell under high cross-linker concentrations. F-actin is not only of biological importance but also, as an example of a semiflexible polymer, has attracted significant interest in its physical behavior. In combination with different cross-linkers semiflexible filaments may provide new routes to bio-materials development and act as the inspiration for new hierarchical network-based materials.

I. INTRODUCTION

Actin is a major component of the cell cytoskeleton and in the eukaryotic cell this protein exists in two forms, globular (G-actin, single protein units) and filamentous (F-actin, a long helical assembly of G-actin monomers) [1]. F-actin is an interesting molecule for both physicists and biologists as it has a very large length-to-width ratio but remains relatively stiff (persistence length ~ 10 μm) [2,3]. This property makes F-actin an excellent example of a semiflexible filament and, due to its relatively large size (7 nm in width), the physical behavior of this class of molecules can be easily probed in solution using fluorescence-imaging techniques. The structure and properties of materials generated from semiflexible filaments have not been investigated in anywhere near the detail that has been devoted to flexible polymer structures and this is an area of research with great potential for the future in materials science. With the development of artificial semiflexible polymer systems, F-actin will provide the inspiration for the development of new hierarchical networks and gels.

Over the past decade considerable work has clarified that F-actin, under different solution conditions, forms differently ordered structures [4–30]. For example, in the presence of counterions or linking proteins of small size, such as fascin, F-actin forms tight-binding straight individual bundles [4–10]. On the other hand, F-actin in the presence of large and more flexible linking proteins will assemble into more interesting complex structures, such as networks of filaments and bundles [11–25,31–33]. The morphology of these networks results from not only the shape of the cross-linker but also the exact nature of the cross-linker. In the presence of α-actinin, F-actin filaments pack together into a ladderlike bundle structure on the nanoscale, and at high cross-linker:actin molar ratios F-actin filaments will assemble into a fascinating hierarchical network of filament bundles [11,14,15]. Although studies have been devoted to elucidation of self-assembly mechanisms, it is clear that the high cross-linker ratio regime for semiflexible filaments is one which is as yet relatively unexplored.

Despite recent progress a complete understanding of the structures and their formation mechanisms in this system is still lacking, particularly for assembled systems under extreme conditions, such as very high concentrations of cross-linking proteins. High localized concentrations of cross-linking proteins can be found in healthy cells and are typically present in filapodia or the stress fibers. In recent years there have been several studies linking overexpression of cross-linking proteins to different cancers. The excess formation of cellular protrusions is linked to metastasis of cancer cells as it promotes cellular protrusion formation and therefore cell spreading [34–37]. In addition, some work has been carried out on the use of cross-linker overexpression in tumor suppression [34,38]. With this current interest it is important to undertake a fundamental study of the behavior of cross-linking proteins at high concentrations to aid the interpretation of biological data.

In this article we report a detailed investigation of the mechanisms behind the hierarchical assembly of actin bundle networks on a wide range of different cross-linking concentrations from low concentrations, crossing over into the regime where there is more than one cross-linker per G-actin in the solution. Intuitively one might expect no changes in structure beyond this limit; however, this is not the case and several interesting structural changes in the macroscopic network take place above this point. Our work combines confocal fluorescence imaging of actin bundle networks with coarse-grained molecular dynamics simulation over a wide phase space. Using confocal microscopy, we show that at cross-linker:G-actin $\geqslant$ 1:1 three different bundle network regimes can be identified. Our data demonstrate that the assembled bundle network system can fall into one of three different regimes: (a) a loosely connected network of F-actin and bundles (as reported previously [16]), (b) a dense uniform network of bundles, and, interestingly, (c) a loosely connected network of dense domains—an intermediate regime between the first two. The phenomena can be explained by qualitatively considering the assembly mechanism. The formation of the bundle network is recovered in our simulation model by

primarily considering Coulombic interactions as an attractive potential between filaments and cross-linkers. In previous work [16] it has been shown that the formation of the network of bundles can be explained by a cluster-cluster aggregation of branched bundles in the diffusion limited aggregation (DLA) regime. The network is locked into a structure out of equilibrium by strong cross-linker binding.

Although the α-actinin–F-actin system has been studied by Hirst in some detail at high cross-linker concentrations [16], little research has been carried out on other cross-linkers in this regime. To this end we have also carried out simulations with different types of cross-linkers to represent the proteins, fascin and filamin. Using the same simple potentials we observe single-filament networks at low concentrations of a model filamin cross-linker, filament bundle networks at high concentrations of filamin, and filament bundles in the presence of fascin. We observe structures comparable with those observed experimentally, including filamin bundling [23]. These results, demonstrate that network architecture in semiflexible filament systems can be controlled by both cross-linker morphology and binding configuration on the actin filament.

By utilizing molecular dynamics (MD) simulation [39] as a complementary technique to experimental fluorescence microscopy we are able to investigate the full range of important length scales in this system. Fluorescence microscopy is an excellent probe for length scales above the optical resolution limit ($\sim$200 nm). However, much of the interesting self-assembly takes place below this threshold, including the binding of cross-linking proteins to the actin filament and the details of the bundle structures as well as the connected network. It is, of course, possible to probe submicron length scales with other experimental techniques; however, there are various limitations to these techniques that do not give the full picture. Scattering and diffraction techniques provide an ensemble measurement on small length scales but no information on intermediate to large length scales. Transmission electron microscopy (TEM) can be more informative, but typically the samples are no longer in their free 3D state in solution. The networks we are investigating have a hierachical structure ranging from nanometer to millimeter length scales so, in order to examine the structure *across length scales*, simulation is very valuable. We are able to look at what is happening at branch points and how that can correlate with cross-linker arrangement inside the bundles.

II. MATERIALS AND METHODS

A. Protein preparation and fluorescence microscopy

For confocal microscopy G-actin (Cytoskeleton, Inc., Denver, CO) labeled with Alexa Fluor 488 conjugate G-actin from rabbit muscle (Invitrogen, Carlsbad, CA) is polymerized into F-actin at 10 μM in F-buffer (5 mM Tris-HCl, 0.2 mM CaCl$_2$, 50 mM KCl, 2 mM MgCl$_2$, 1.2 mM ATP, 0.5 mM DTT). F-actin filament length is controlled by the presence of gelsolin during polymerization [40]. After 2 h of actin polymerization, phalloidin is added with a 1:1 molar ratio to stabilize F-actin and prevent F-actin length change due to depolymerization. α-Actinin (Cytoskeleton, Inc.) was suspended in 20 mM NaCl,

1 mM β-mercaptoethanol, 20 mM Tris-HCl (pH 7.2), 5% sucrose, and 1% dextran buffer and added to the F-actin solution to induce assembly. The concentrations of actin and α-actinin:actin molar ratio are varied for different assembled network structures which are observed using fluorescence confocal microscopy. Actin concentrations were chosen in this study $\sim$0.5 μM to mimic concentrations typical for actin in the cytosol of nonmuscle cells.

B. Fluorescence confocal microscopy

Actin networks were prepared by depositing a 2-μl droplet of F-actin solution on a welled glass slide and then adding a droplet of cross-linker solution to the droplet, taking care to keep the buffer conditions optimal for the proteins and controlling the molar ratio of cross-linker to G-actin. The protein solutions were not mechanically mixed and therefore diffusion of the cross-linker through the F-actin solution was the primary mechanism for combining the two proteins. The droplets were sealed into the welled glass slide by a thin glass cover slip, just making contact with the upper surface of the droplet. Laser-scanning confocal microscopy was carried out on a Nikon TE-2000U with an excitation wavelength of 488 nm.

C. Molecular dynamics simulation

In order to carry out molecular dynamics simulations on such a massive system, we model F-actin as a chain of 50 beads separated by 20 nm, each of which has a mass equivalent to 7 G-actins and carries a negative charge of $-14e$ ($-2e$ per G-actin). Note that, experimentally, the assembly of F-actin in the high cross-linker regime has been studied with a variety of the average F-actin lengths, from 300 nm [15,16] to 21 μm [22,23]. Within this range of lengths minimal qualitative effects on the assembled structure have been observed, primarily a change in the mesh size of the network. The detailed effects of length in this regime have yet to be quantified systematically. Our experimental results show that there is a very small difference in the assembled network structure, if the F-actin length is controlled to an average length of 1000 nm compared with no length control. It should also be noted that in this simulation the filaments are static, i.e., they are not actively polymerizing or depolymerizing. In our simulations, different cross-linkers are modeled, including α-actinin, filamin, and fascin (Fig. 1). α-Actinin is composed of two positively charged and three negatively charged beads. Filamin is modeled by two branches joining at a charge-neutral bead to form a $\sim$180-nm-long V shape; each branch has two
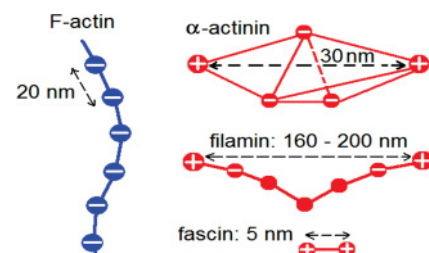

FIG. 1. (Color online) Schematics for the coarse-grained models for F-actin and the cross-linkers: α-actinin, filamin, and fascin.

charged beads and one charge-neutral bead. Fascin includes two positively charged beads connected by a 5-nm-long rod. The details of interaction potentials are described in our previous report, including Coulomb potential of the charges, Van der Waals interactions between close beads, bending energy of the actin filament and filamin, and elasticity of the connecting rods [11]. At the beginning, F-actin and cross-linkers are put randomly in a cubic box 4000 nm in size. Periodic boundary conditions are used for all three dimensions. Molecular dynamics simulations are run up to 1000 ns and the equilibrium of the system in confirmed by investigating the energy curve.

III. RESULTS AND DISCUSSION

A. Molecular dynamics simulation of F-actin networks

Molecular dynamics simulations were initially carried out on a system of F-actin filaments with a cross-linker modeled to represent α-actinin. Figures 2(a)–2(c) show several snapshots of the assembled system. In the snapshots, F-actin is visualized as blue (light gray in print) and the cross-linker as red (dark gray in print). N_{FA} denotes the number of actin filaments in the system, and γ denotes the equivalent linker-to-G-actin molar ratio. The cross-linker was designed specifically to mimic the binding behavior of α-actinin with binding between two filaments at a high angle to give a ladderlike structure [14,15]. This was achieved by tuning the magnitude of the different charges on the molecular model, and close inspection of the simulation visualizations confirmed the expected binding behavior. We find that a macroscopic model for the cross-linker is sufficient to capture networking behavior and that, particularly in the case of larger cross-linkers where the filament spacing is much larger that the Bjerrum length (0.71 nm in water), it is not necessary to consider the effects of salts in the solution. Figures 2(a)–2(c) show a magnified small region to give a representative view of the binding between F-actin and cross-linkers and the overall network structure. We can clearly see that a variety of network structures can occur depending on the initial concentrations of actin and the cross-linker (N_{FA} and γ). At $\gamma = 0.16$, $N_{FA} = 500$ [Fig. 2(a)] we see individual actin filaments connected by few cross-linkers. Figure 2(b) shows filaments branching out from a bundle to connect with single filaments at $\gamma = 0.27$, $N_{FA} = 750$, and Fig. 2(c) demonstrates bundles branching out from a larger bundle to form a strongly connected network at $\gamma = 0.36$, $N_{FA} = 1000$. 3D visualization combined with Fourier analysis shows that a given assembled system can be classified into one of three different structures: a loosely connected network of individual actin filaments [Fig. 2(a)], a network composed of a mixture of filaments and bundles [Fig. 2(b)], or a network of strongly connected branching bundles [Fig. 2(c)]. Each of these regimes corresponds well with structures that have been observed experimentally for α-actinin networks [13,15,20].

B. Structural analysis of simulated networks

To provide a more quantitative analysis of the simulation results for each network and to investigate the average structural properties in more detail we calculated the Fourier transform of the mass density for each assembled system.
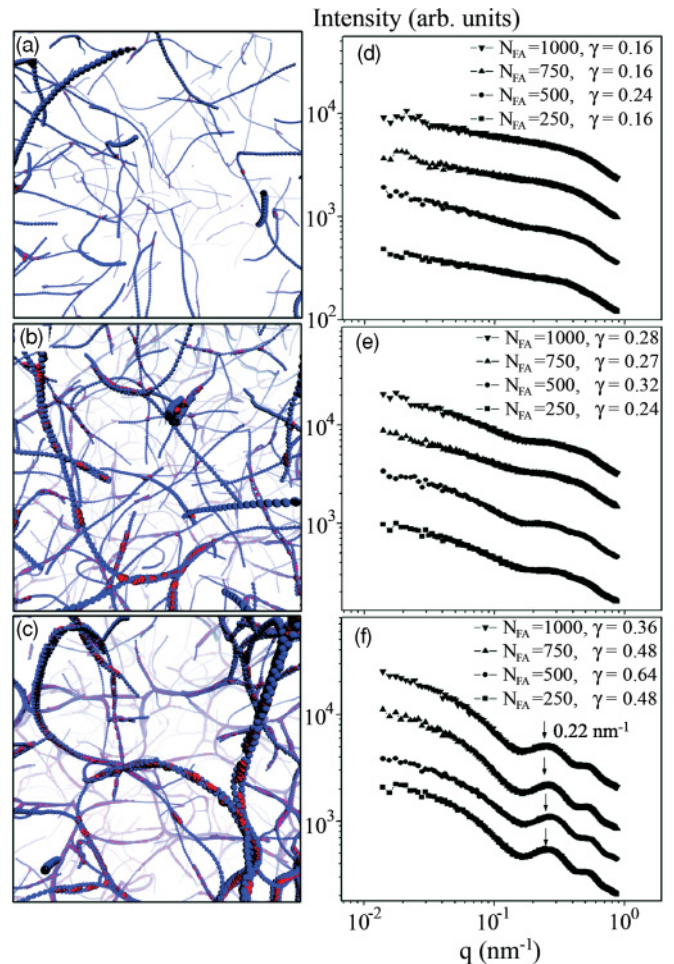

FIG. 2. (Color online) Molecular dynamics simulation snapshots of different binding configurations (red (dark grey) dots represent cross-linkers): (a) connected network of filaments, $N_{FA} = 500$, $\gamma = 0.16$; (b) composite network of filaments and bundles, $N_{FA} = 750$, $\gamma = 0.27$; (c) branching network of bundles, $N_{FA} = 1000$, $\gamma = 0.36$. [(d), (e), and (f)] The intensity curves of the Fourier transform of the mass density calculated for (d) connected networks of filaments, (e) composite networks of filaments and bundles, and (f) branching networks of bundles.

Using this method one can characterize the average internal structure of the simulated bundles for small length scales and also obtain quantitative data on the global properties of the assembled system.

3D Fourier transform is calculated as $F_k = \int_{Vol} D(\boldsymbol{r}) e^{ikr} d^3 \boldsymbol{r}$, where D is the mass density of the system. The intensity of the power spectrum $[I(q)]$ is then given by, $I(q) \propto \int_{S(q)} |F_k|^2 dS_k$, where $S(q)$ is a spherical surface of radius q. Figures 2(d)– 2(f) show the results of this calculation with different combinations of N_{FA} and γ. We observe clear variations in network characteristics by plotting intensity I versus q.

For networks of individual actin filaments [i.e., at low cross-linker concentrations ($\gamma \leqslant 0.24$)], the Fourier transform intensities show a monotonically decreasing behavior [Fig. 2(d)]. The curve is linear down to $\sim$20 nm (the filament bead spacing) with a $\sim q^{0.3}$ behavior and this low dimensionality can be explained as a result of the coarse-grained model,

constructed of effectively point masses connected by mass-less springs. As the concentration of cross-linkers in the system increases [Fig. 2(e)] and denser structures form, this exponent increases as expected, although the exact value is difficult to determine due to the appearance of other features related to the structure. For systems composed of a mixture of bundles and single filaments ($\gamma = 0.24$–0.32), we observe small bumps in the intensity curves [Fig. 2(e)]. Finally, more defined Bragg peaks are clearly shown in the case where the system is composed of a network of branched bundles [Fig. 2(f)]. In the case of networks of individual filaments, the filaments are quite randomly oriented, showing no ordered structure. On the other hand, the clear peaks on the intensity curves in the case of the networks of bundles represent the internally ordered structure of the bundles that can also be seen in the 3D visualization [Fig. 2(c)] and is analogous to Bragg scattering. The internal ordering of actin bundles in this regime has been previously determined experimentally in vitro [15]. In our simulation the Fourier transform characterizes filament packing inside the bundle as being consistent with this data. The peak indicates a characteristic spacing between parallel filaments. The appearance of the first peak at the same position in q for different numbers of filaments and cross-linker:actin molar ratios in the system indicates that the ladderlike structure of formed bundles is well defined primarily by the ability of the cross-linker to bind to filaments at high angles. The position of this peak corresponds to $q = 0.22$ nm^{-1} or a filament spacing of 29 nm, a distance representative of the length of the cross-linker [15]. Now by using a combination of 3D visualization and Fourier transform analysis of the mass density, we can easily categorize the assembled systems into three groups: (i) with no evidence of macromolecular structure formation in the Fourier transform data, (ii) small bumps in the Fourier transform intensity curves, and (iii) with the quasi-Bragg peak clearly seen in the Fourier transform data. To quantify our classification, we calculate the number of bound actin beads in each simulated assembled system and find that, for networks with no peaks on the Fourier transform intensity curves, the percentage of bound actin beads (P) is between 1% and 15%; for networks showing small bumps on the Fourier transform intensity curves, P is between 22% and 47%; and for networks with a clearly shown quasi-Bragg peak, P is between 60% and 81%. In Fig. 3(a) these results are presented for a variety of different simulated networks in which we vary the total number of filaments in the system (N_{FA}) and the ratio, γ. Each data point represents a simulated network and the color is assigned based on our network classification method described above. These results show that the properties of the assembled systems depend strongly on the linker-to-actin molar ratio γ and slightly on the actin density (here represented by the number of actin filament N_{FA}). The diagram shows the onset of bundle formation at $\gamma \simeq 0.25$ which changes only slightly with N_{FA}. This ratio is in good agreement with experimental data for the bundling transition threshold of 0.2 [20]. We observe the network of branching bundles starting to form at γ within the range of 0.35–0.4. Experimentally [16], more rigid gel-like properties were observed above $\gamma = 1$; however, fairly well-defined networks were observed at lower γ values so this simulation provides a good estimate for the threshold of bundle network formation.
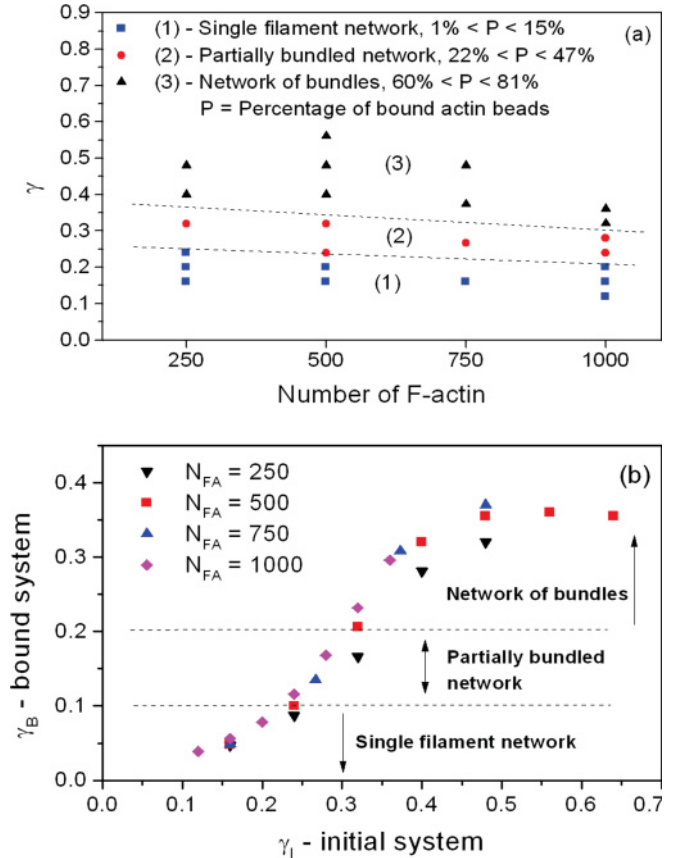

FIG. 3. (Color online) Schematic for categorized groups of simulated α-actinin–F-actin structures. Each point represents a data set and the dotted lines are a guide to the eye. (a) Behavior with increasing cross-linker to actin molar ratio (γ_I) as the total number of actin filaments in the system is increased. (b) The relationship between $\gamma_I = \gamma$ and the ratio of bound cross-linkers to total actin filaments (γ_B).

One additional factor that must be taken into account in estimating this threshold is the dissociation rate of α-actinin after binding to the actin filament [41]. We expect this to have some effect on the threshold for the formation of the network of bundles and will be incorporated into the model in the future. At very high cross-linker ratios there will be a considerable amount of binding redundancy in the formation of the structure, therefore the effect will be lessened.

In addition to the structure categorization in Fig. 3(a), we calculated the molar ratio of bound cross-linkers to actin (γ_B) and plot this parameter as a function of the total linker-to-actin molar ratio for the initial system (γ_I, equivalent to γ in other figures) to show how the degree of binding is dependent on the overall number of cross-linkers in the system for different actin densities [Fig. 3(b)]. To calculate this we removed all filaments and cross-linkers which were not bound to any other filament or cross-linker in the system after it was equilibrated, leaving behind only the bound filaments and cross-linkers. In Fig. 3(b), for group 1 (networks of individual filaments), γ_B falls within the range of 4%–9%; for group 2, (composite network of filaments and bundles), γ_B falls within the range of 10%–21%; and for group 3 (networks of bundles), γ_B falls within the range of 24%–37%. The results demonstrate that

γ_B is not only a function of γ_I but also depends slightly on the initial number of F-actin N_{FA}. This is expected because varying the density of F-actin (represented by N_{FA}) will vary the chance for a cross-linker to meet and bind to an F-actin. A consistent conclusion will be drawn from our experimental study presented below.

C. Varying linker morphology

In order to probe the effects of cross-linker morphology on network structure, we have carried out simulations, varying the type and concentration of linking agent. In addition to the "α-actinin-like" cross-linker described earlier, we have also designed a "filamin-like" linker and a "fascin-like" linker. Figure 4 shows results for the F-actin simulation with different types of linker at low and high concentrations: Figs. 4(a) and 4(b) for α-actinin, Figs. 4(c) and 4(d) for filamin, and Figs. 4(e) and 4(f) for fascin.

In the F-actin–α-actinin system, at a low linker-to-actin molar ratio (γ) [Fig. 4(a)], a network of single filaments forms. At high γ [Fig. 4(b)] the structure can be described as a branching network. That is, larger bundles branch out into smaller bundles. These small bundles, then, on joining with other bundles, become a part of other larger bundles.
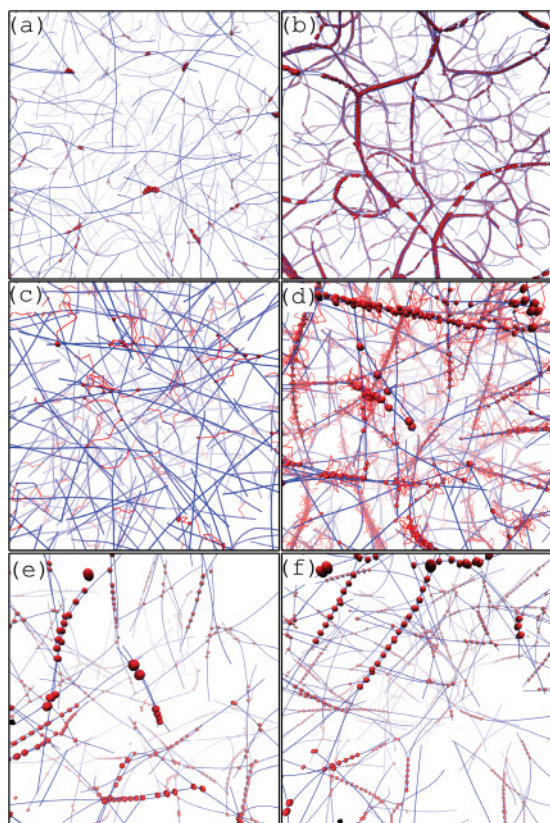

FIG. 4. (Color online) Molecular dynamics simulation snapshots for an F-actin coarse-grained system with different cross-linker types (red (dark grey) dots represent cross-linkers) at low and high linker-to-actin molar ratios. For α-actinin: (a) $\gamma = 0.16$, $N_{FA} = 500$ and (b) $\gamma = 0.36$, $N_{FA} = 1000$; for filamin: (c) $\gamma = 0.04$, $N_{FA} = 500$ and (d) $\gamma = 0.1$, $N_{FA} = 500$; for fascin: (e) $\gamma = 0.02$, $N_{FA} = 500$ and (f) $\gamma = 0.045$, $N_{FA} = 500$.

Thus the network fills three-dimensional space by continuous branching. In a previous recent study [11] evidence was found that a combination of two factors lead to this unique branched network. These are the extended size of the cross-linker ($\sim$35 nm in the case of α-actinin) and the semiflexibility of the F-actin filament. These factors both provide favorable conditions for bundle branching. It was also observed that by constraining the F-actin into branching ladderlike bundles, high curvature in the system can become "locked in." We observe that the system of F-actin and a "filamin-like" linker is also capable of forming a branching network of bundles, although the binding configuration of the cross-linker differs slightly. At low concentrations, the flexible cross-linker takes a high "V" angle to create a single filament network [Fig. 4(c)]; however, at high concentrations bundles will form [Fig. 4(d)]. The bundles are connected by the linkers to form a network. This transition in the filamin system has been observed experimentally at $\gamma \simeq 0.1$ [23], although the exact binding configuration inside the bundle is not known.

In contrast to the "locked-in" network observed in the α-actinin–actin system, the bundles in the filamin-actin system are loosely connected to each other due the high flexibility of the linker. That is why the bundles appear to be quite straight with low curvatures in contrast to the high curvatures of α-actinin–actin bundles. While the ladderlike structures leave a large gap between F-actin in bundles with α-actinin, flexible filamin does not constrain F-actin in bundles to a wide d spacing. Instead, highly filamin-linked bundles collapse into a disordered tight-binding form. Our preliminary small-angle x-ray scattering on a system of filamin-to-actin molar ratio of 1:9 shows similar characteristics with those of F-actin bundled by divalent counterions of low concentration which has been confirmed to have disordered tight-binding bundle structure [10]. A TEM image of a counterion-induced bundle is shown in Fig. 5.

Like α-actinin, fascin can bundle F-actin into a well-defined structure [5,8]. However, evidence for fascin linking F-actin bundles into a network is weak [17,18]. Our MD simulation results show that due to the small size of the fascin molecule, the F-actin bundles are tightly packed and have very little flexibility to branch out [Figs. 4(e) and 4(f)]. Consequently, most bundles are very straight and a connected network is barely observed. This result is further evidence that a long cross-linker is required for the branching network of bundles.
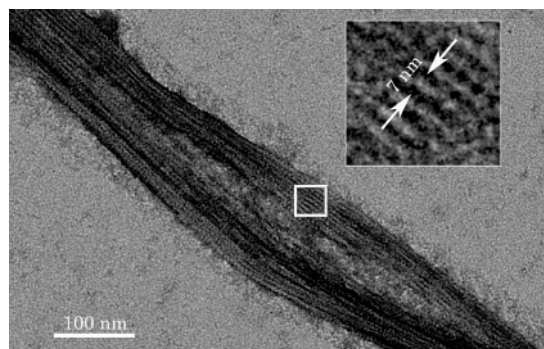

FIG. 5. Transmission electron microscopy image and a magnification of a small area of a closely packed F-actin bundle in presence of 80 mM MgCl$_2$.

It is important to note here that the interactions of counterions within the system are not accounted for in these coarse-grained models as our goal is not to investigate the detailed effects of physiological salts on the system but instead to investigate the roles of cross-linker and filament morphologies on final network formation. Previous investigators [6,10] and our TEM study have shown that F-actin in the presence of divalent counterions forms straight, closely packed bundles (Fig. 5) and branching does not occur. This extreme case provides additional evidence that the formation of a branching network depends not only on the concentration of linking agent but also on the type of the linking agent, as this will determine the filament spacing within the bundle. A bundle with a wider filament spacing will tend to branch more often. This conclusion is also reflected in our simulation results.

D. Fluorescence imaging of actin bundle networks

In order to explore the complete phase space for an assembled system of F-actin and cross-linkers, several parameters can be varied, including actin concentration (C_A), cross-linker-to-G-actin molar ratio (γ), and cross-linker type. In this article we have looked at each of these using simulation, but, in addition, fluorescence confocal microscopy can be used to provide additional information, both for large length scales that cannot be easily accessed by our simulation and also to ensure that the simulation studies accurately represent the real system.

Confocal microscopy was carried out on F-actin–α-actinin bundle networks focusing on high γ ratios. This filament–cross-linker system has been investigated previously by this method, revealing the existence of the network of bundles, but here we provide a more detailed analysis of network architectures at high cross-linker ratios. Using confocal microscopy we can visualize the 3D network by taking a series of images at different focal points. Images of the system for different values of C_A and γ are shown in Fig. 6. These images reveal interesting results. Three different bundle network regimes were identified, a loose, low density network of bundles; an inhomogeneous structure with network domains and vacancies; and a higher density network of bundles.

Using fluorescence microscopy, a complication arises in trying to image differently sized actin assemblies simultaneously (especially in 3D): F-actin bundles appear much brighter than single F-actin filaments; therefore, it is not possible to simultaneously image both free single filaments and bound filaments (in bundles) in the same sample. For this reason, it is very useful to have 3D visualization of MD simulation results (which by their nature show the position of every filament in the system) [Fig. 2(a)].

In Fig. 7, experimental data are shown for the three different bundle network structures observed by confocal microscopy and classified by the analysis described in the following section. By comparing data for F-actin with an uncontrolled length [Fig. 7(a)] and data for F-actin with an average length of 1000 nm, controlled by the addition of the actin severing and capping protein gelsolin [Fig. 7(b)], we can see that, within our parameter range, this morphological behavior depends

strongly on γ but weakly on the F-actin length and C_A. This conclusion has also been confirmed from our MD simulation results in which we varied the F-actin length from 400 to 1000 nm in the presence of high cross-linker concentration. These experimental data show that, even at very high γ, different structures are formed from different combinations of C_A and γ: (a) a loose homogeneous network of F actin and bundles that results from a lower C_A and γ, (b) an inhomogeneous domainlike network in which there are many vacancies (an intermediate phase) as C_A and γ increase, and (c) a dense homogeneous network of bundles when C_A and γ are high (in this case the system forms a strongly connected network of F-actin bundles with a smaller mesh size than the first homogeneous network). In regime (a), fewer bundles are observed and this is reflected in the simulation data (shown below for comparison in which a low percentage of F-actin filaments were bound together by cross-linkers). While in regimes (b) and (c), higher percentages of bound F-actin (bundles) are observed. This observation shows that the properties of the assembled system depend on both the actin concentration and molar ratio. However, from the data shown in Fig. 7, we can see that the γ dependence is much stronger than C_A dependence.

To explain the existence of the three high γ regimes, shown in Fig. 6, we can consider the attraction between the F-actin filament and the cross-linker to be dominated by the electrostatic interaction. In a physiological environment the polyelectrolyte like nature of F-actin and its interaction with the surrounding environment (dissolved counterions) create local barrier potentials that tend to keep the system in equilibrium while the interaction between F-actin and the cross-linkers induces aggregation. The dynamics of the self-assembly are governed by a mutual dependence between the protein density distribution and the course of aggregation. The interaction between the F-actin and the cross-linkers is a function that depends on the protein density distribution while the aggregation in return will modify this density distribution. As self-assembly proceeds, the redistribution of density for a more favorable electrostatic energy state takes place and the system gradually reaches a new equilibrium state.

For certain combinations of C_A and γ, two aggregation scenarios can occur: (i) a homogeneous connected network of filaments forms first (high C_A and γ) or (ii) small individual bundles form first (low and medium C_A and γ). Following this primary aggregation, a depletion effect of proteins takes place due to the binding of F-actin wih cross-linkers. At high C_A and γ, a secondary aggregation occurs in which free filaments add to bundles in the network and finally form a strongly connected network of bundles. However, at low C_A and γ, protein is depleted from the solution and the system ends up as a loose network of individual bundles and filaments as the bundles eventually find each other and stick. In the intermediate C_A and γ regime, initial aggregation does not deplete all F-actin and cross-linkers but instead reduces significantly the concentrations of free F-actin and cross-linkers compared to those in the bound regions. As a result, the bound F-actin and cross-linker regions become attraction centers due to their relatively high densities and then attract more free F-actin and cross-linkers to become denser. This breaking of homogeneous
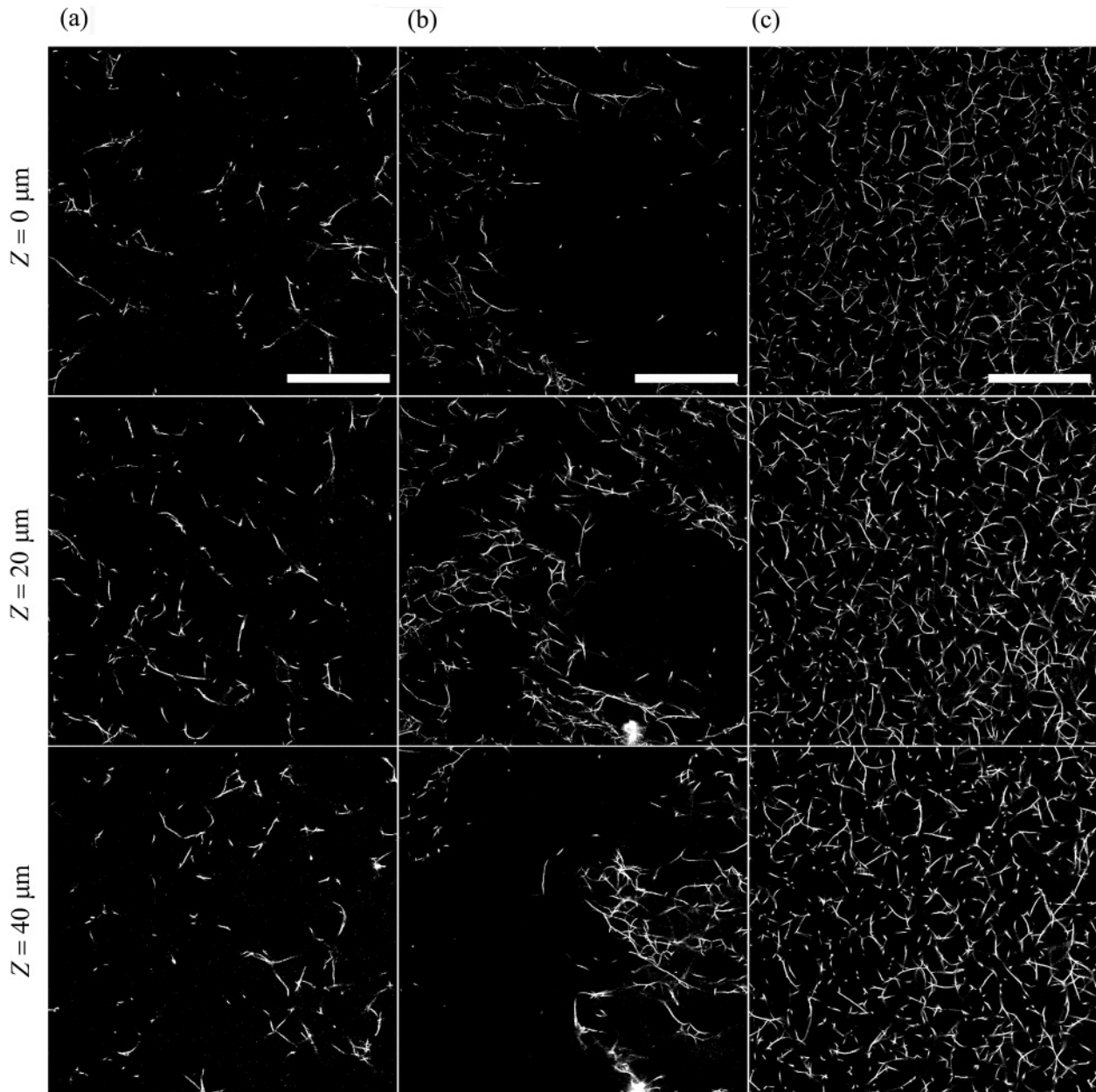
FIG. 6. Laser-scanning fluorescence confocal images of α-actinin–F-actinin networks at high cross-linker concentrations. (a) A loose network of bundles $C_A = 0.3$ μM, $\gamma = 1.0$; (b) large gaps in the network are observed $C_A = 0.6$ μM, $\gamma = 1.0$; (c) a dense network of bundles $C_A = 1.2$ μM, $\gamma = 2.0$. Scale bars denote 50 μm.

distribution of F-actin and cross-linkers results in the formation of domains.

E. Structural characterization of real 3D networks imaged by confocal microscopy

To study length scales in the 3D networks imaged using confocal microscopy (at $\gamma \geqslant 0.25$), we carry out an analysis in which we characterize the distribution of mass in the network as a function of length scale. This allows us to identify any well-defined mesh sizes in the system. Each confocal data set is composed of a stack of images providing a 3D fluorescence image of the network down to the resolution limits of the microscope. Therefore, by using fluorescence intensity to represent mass we essentially have a 3D mass matrix of the system. To investigate network homogeneity on a particular length scale we divide the whole system into a series of cubic blocks of the same volume and compare their masses. The standard deviation (σ) of the block mass is calculated and normalized as $\rho = \sigma/\mu$, where μ is mean block mass. This calculation is repeated for a range of different block sizes, and then ρ is plotted versus the block size (Fig. 8). A large standard deviation in block mass for a particular block size indicates that some blocks contain a lot of actin and others contain very little, therefore we expect inhomogeneity on that length scale. If every block of a particular size contains approximately the same mass then the network is homogeneous on that length scale. In general, a homogeneous system yields a small ρ
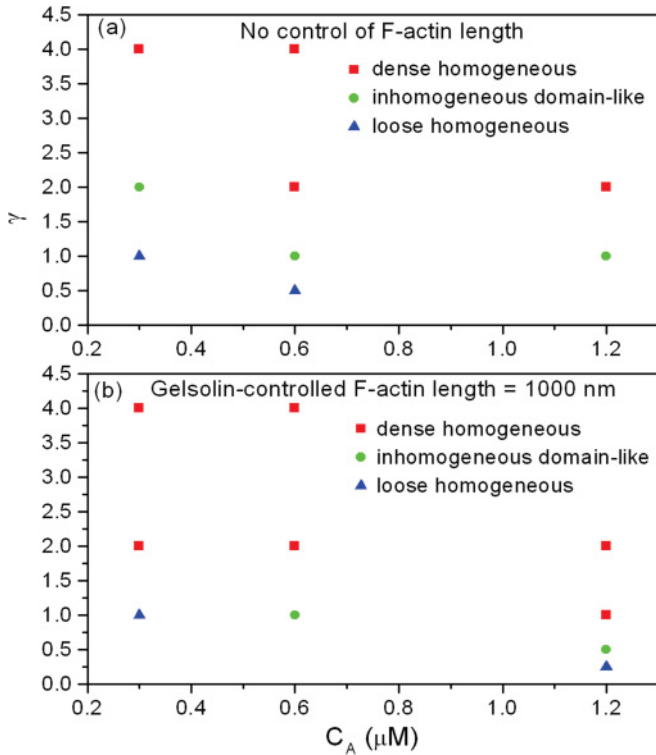
FIG. 7. (Color online) Experimental "phase diagram" constructed from confocal fluorescence microscopy data in the high cross-linker ratio regime. Data are shown for F-actin networks in the presence of α-actinin, varying actin concentration (C_A) and the α-actinin–G-actin molar ratio (γ). (a) No control of F-actin length and (b) F-actin lenght is controlled by the addition of gelsolin to be ~1000 nm.

and an inhomogeneous one yields a large ρ. This technique can be used to quantify the macroscopic characteristics of our 3D network structures quite effectively, as shown in Fig. 8.

In all the systems shown in Fig. 8, when the block size is chosen less than ~10–15 μm, ρ is large. This behavior reflects the fact that the system is not homogeneous below the length scale of the mesh size and is expected. As the block size for analysis is increased to close to the mesh
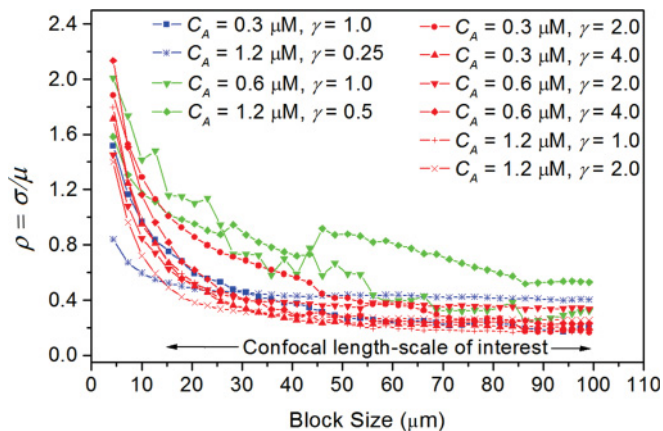

FIG. 8. (Color online) Ratio of the standard deviation to average mass as a function of block size calculated for different filament–cross-linker concentrations from confocal fluorescence microscopy data.

size, the mass density changes dramatically, giving rise to the sharp change in ρ. From this we can estimate the mesh size of the system to be about 15 μm—the size at which we transition from a microscopic view to a macroscopic view. If the block size is larger than the mesh size, we see various ρ behaviors for different network structures. The (lower) blue and red curves representing homogeneous network structures [Figs. 6(a) and 6(c)] decrease slightly and smoothly through the whole range. This is due to the fact that, in a homogeneous system, the mass density varies only slightly for any given length scale, giving rise to small differences in block mass and, hence, small mass standard deviation. When the block size increases, the relative difference in block masses decreases slightly, resulting in the smoothly decreasing behavior of ρ. On the other hand, the (upper) green curves, which represent inhomogeneous domainlike structures [an example of which is shown in Fig. 6(b)], show a discontinuous change in ρ in a range from 15 to 60 μm. This change reflects the inhomogeneous characteristics of the structure, as the significant difference in block masses yields a large deviation. We see that for these curves, when the block size increases to more than 60 μm, ρ becomes smooth. This indicates that the average separation of the domains is ~60 μm.

IV. CONCLUSION

In this article we have used MD simulations and fluorescence microscopy to demonstrate the interesting novel structures that can be formed by F-actin in the presence of different cross-linkers by varying concentrations of the protein components. A Fourier transform analysis of simulated α-actinin–F-actin networks was used to categorize different network structures with respect to two parameters, linker-to-actin molar ratio and actin concentration, showing that the structure depends strongly on the former but weakly on the latter. We also present preliminary simulation results for two other cross-linkers designed to model filamin and fascin. At high simulated cross-linker concentrations our results suggest that cross-linker shape strongly influences whether we see a network of bundles, as previously observed experimentally [30], and this will be a rich area for future investigation. Simulation will allow us to subtly modify cross-linker structure and probe the effects of these changes on network properties. Confocal fluorescence microscopy observation of real 3D networks formed by F-actin in the presence of α-actinin revealed new behavior in which three structural regimes were defined in the high α-actinin–actin molar ratio limit ($\gamma = 0.25$–4) while actin concentration and F-actin length were also varied. This observation was quantified by a length-scale analysis to show that the assembled structure depends on γ, actin concentration, and filament length. The data presented in this article demonstrate the tunability of the F-actin system across length scales from the internal bundle structure to large-scale network morphology. Macroscopic tunability based on nanoscale structure is a promising route to the synthesis of novel bio-inspired materials, and studies of such systems benefit from a combined approach using simulation and experimental work, as it is difficult to fully characterize hierarchical networks at length-scales between

50 nm and 1 μm. These results and previous evidence suggest that a large cross-linker combined with the semiflexible filament with a persistence length on the length scale of the mesh size are required to generate the network of bundles. Our simulation will be ideal to probe this idea systematically and future work in varying filament flexibility will be an important goal.

[1] H. Lodish, A. Berk, C. A. Kaiser, and M. Krieger, *Molecular Cell Biology*, 4th ed. (Freeman, New York, 1999).

[2] J. Käs, H. Strey, M. Bärmann, and M. Sackmann, Europhys. Lett. **21**, 865 (1993).

[3] A. Ott, M. Magnasco, A. Simon, and A. Libchaber, Phys. Rev. E **48**, 1642 (1993).

[4] J. Tang and P. Janmey, J. Biol. Chem. **271**, 8556 (1996).

[5] L. Haviv, N. Gov, Y. Ideses, and A. Bernheim-Groswasser, Eur. Biophys. J. **37**, 447 (2008).

[6] H. J. Kwon, A. Kakugo, K. Shikinaka, Y. Osada, and J. P. Gong, Biomacromolecules **6**, 3005 (2005).

[7] M. M. A. E. Claessens, C. Semmrich, L. Ramos, and A. R. Bausch, Proc. Natl. Acad. Sci. **105**, 8819 (2008).

[8] J. Bryan and R. E. Kane, J. Mol. Biol. **125**, 207 (1978).

[9] J. J. Otto, R. E. Kane, and J. Bryan, Cell **17**, 285 (1979).

[10] T. E. Angelini, H. Liang, W. Wriggers, and G. C. L. Wong, Proc. Natl. Acad. Sci. **100**, 8634 (2003).

[11] L. T. Nguyen, W. Yang, Q. Wang, and L. S. Hirst, Soft Matter **5**, 2033 (2009).

[12] R. Meyer and U. Aebi, J. Cell Biol. **110**, 2013 (1990).

[13] D. H. Wachsstock, W. H. Schwarz, and T. D. Pollard, Biophys. J. **65**, 205 (1993).

[14] K. A. Taylor, D. W. Taylor, and F. Schachat, J. Cell Biol. **149**, 635 (2000).

[15] O. Pelletier, E. Pokidysheva, L. S. Hirst, N. Bouxsein, Y. Li, and C. R. Safinya, Phys. Rev. Lett. **91**, 148102 (2003).

[16] L. S. Hirst, R. Pynn, R. Bruinsma, and C. R. Safinya, J. Chem. Phys. **123**, 104902 (2005).

[17] Y. Tseng, E. Fedorov, J. M. McCaffery, S. C. Almo, and D. Wirtz, Mol. Biol. **310**, 351 (2001).

[18] O. Lieleg, M. M. A. E. Claessens, C. Heussinger, E. Frey, and A. R. Bausch, Phys. Rev. Lett. **99**, 088102 (2007).

[19] G. Z. Sowa, D. S. Cannell, A. J. Liu, and E. Reisler, J. Phys. Chem. B **110**, 22279 (2006).

[20] M. Tempel, G. Isenberg, and E. Sackmann, Phys. Rev. E **54**, 1802 (1996).

[21] M. L. Gardel, F. Nakamura, J. H. Hartwig, J. C. Crocker, T. P. Stossel, and D. A. Weitz, Proc. Natl. Acad. Sci. **103**, 1762 (2006).

[22] O. Lieleg *et al.*, Soft Matter **5**, 1796 (2009).

[23] K. M. Schmoller, O. Lieleg, and A. R. Bausch, Biophys. J. **97**, 83 (2009).

[24] J. H. Hartwig and T. P. Stossel, J. Mol. Biol. **145**, 563 (1981).

[25] I. Borukhov, R. F. Bruinsma, W. M. Gelbart, and A. J. Liu, Proc. Natl. Acad. Sci. **102**, 3673 (2005).

[26] A. Michelot *et al.*, Curr. Biol. **16**, 1924 (2006).

[27] M. Hosek and J. X. Tang, Phys. Rev. E **69**, 051907 (2004).

[28] H. Fazli and R. Golestanian, Phys. Rev. E **76**, 041801 (2007).

[29] P. Kraikivski, B. M. Slepchenko, and I. L. Novak, Phys. Rev. Lett. **101**, 128102 (2008).

[30] O. Lieleg, M. M. A. E. Claessens, and A. R. Bausch, Soft Matter **6**, 218 (2010).

[31] Y. Ideses, Y. Brill-Karniely, L. Haviv, A. Ben-Shaul, and A. Bernheim-Groswasser, PLoS ONE **3**, e3297 (2008).

[32] Y. Brill-Karniely, A. B.-G. Y. Ideses, and A. Ben-Shaul, Chem. Phys. Chem. **10** (2009).

[33] H. Shin, K. R. P. Drew, J. R. Bartles, G. C. L. Wong, and G. M. Grason, Phys. Rev. Lett. **103**, 238102 (2009).

[34] J. Menez *et al.*, Oncogene **23**, 2630 (2004).

[35] K. Honda *et al.*, J. Cell Biol. **140**, 1383 (1998).

[36] D. Qualtrough, K. Singh, N. Banu, C. Paraskeva, and M. Pignatelli, Br. J. Cancer **101**, 1124 (2009).

[37] Y. Hashimoto *et al.*, Clin. Cancer Res. **11**, 2597 (2005).

[38] U. Gluck, D. J. Kwiatkowski, and A. Ben-Ze'ev, Proc. Natl. Acad. Sci. USA **90**, 383 (2005).

[39] T. Schlick, *Molecular modeling and simulation: an interdisciplinary guide* (Springer-Verlag, New York, 2000).

[40] P. A. Janmey, J. Peetermans, K. S. Zaner, T. P Stossel and T. Tanaka, J. Biol. Chem. **261**, 8357 (1986).

[41] J. Xu, D. Wirtz, and T. D. Pollard, J. Biol. Chem. **273**, 9570 (1986).